NUCLEAR INSTRUMENTS AND METHODS 169 (1980) 185-198; © NORTH-HOLLAND PUBLISHING CO.

HIGH PRECISION TIME-OF-FLIGHT MEASUREMENTS OF NEUTRON RESONANCE ENERGIES IN CARBON AND OXYGEN BETWEEN 3 AND 30 MeV

S. CIERJACKS[1], F. HINTERBERGER[2], G. SCHMALZ*[1], D. ERBE[1], P.v. ROSSEN[2] and B. LEUGERS[1]

[1] *Kernforschungszentrum Karlsruhe GmbH, Institut für Angewandte Kernphysik II, 7500 Karlsruhe, Postfach 3640, FRG*
[2] *Institut für Strahlen- und Kernphysik der Universität Bonn, Nußallee 14-16, 5300 Bonn, FRG*

Received 10 August 1979

An essentially improved time-of-flight device has been set up at the Karsruhe isochronous cyclotron. Transmission measurements on carbon and oxygen in the energy range from 3–30 MeV with a spectrometer resolution of 5.5 ps m^{-1} allowed neutron resonance energies of some narrow resonances to be determined with an accuracy of 1.2×10^{-5}. The present results are in many cases more accurate than previously published values by more than two orders of magnitude. Above 10 MeV measured excitation energies of various $T=\frac{5}{2}$ states in ^{17}O have an order of magnitude higher accuracy than the most precise determinations from charged particle reactions. Resonance energies and widths of narrow neutron resonances are presented and two sets of data suitable as high precision energy standards are proposed. For the ^{16}O+n system energies and total widths are given of four $T=\frac{3}{2}$ states in the range $7\leqslant E_n\leqslant11$ MeV.

1. Introduction

Various measurements of reliable nuclear data and many nuclear reaction experiments require an accurate knowledge of the incident projectile energies. Frequently it is sufficient to use one or a few precise energy standards to which the measured excitation functions can be normalized. This applies, for instance, to some time-of-flight-systems for which no absolute time-zero point can be determined or for which absolute length and time measurements are difficult to perform. A typical example of the first kind is the energy measurement with an electron linear accelerator providing neutrons from the primary target. In this case neutron detectors are highly overloaded by the intense gamma-flash from the target, and detector voltages must be switched off during prompt gamma-ray arrival times; thus preventing their use as a time-zero reference. But also in cases where this problem does not exist, large neutron source volumes often prevent precise length, and thereby, energy assignments. Large source volumes are, in particular, unavoidable when essential moderation of primary neutron spectra is necessary. Precise energy standards can, therefore, help to ensure that various neutron facilities produce data on the same energy scale and solve existent discrepancies in energy assignments of which several examples have been identified in the past[1]). From the viewpoint of neutron standards, carbon and oxygen are favourable elements in the MeV range since their total cross sections exhibit a large number of isolated narrow resonances. In addition, suitable transmission samples are readily available in elemental form as graphite and liquid oxygen.

There are various methods for the determination of absolute projectile energies. Restricting considerations to neutron beams, an often used alternative to the time-of-flight method is the reaction threshold method[2]). It can be applied when monoenergetic neutrons are produced with electrostatic accelerators. The principle of the method is to measure yield curves preferably of (p, n) reactions at 0° and to extrapolate the data to zero yield. Even though careful extrapolation procedures have been applied, the accuracy of the final results is sometimes severely limited.

Another important method is the energy determination of monoenergetic neutrons by means of charged particle energies involved in the source reaction[3]). In this method, charged particle energies are calculated from the magnetic induction and the curvature of the particle trajectories in an analyzing magnet. While magnetic inductions can, in principle, be determined with high precision by the magnetic nuclear resonance method the main difficulties arise from the relatively large inhomogeneities along particle trajectories and the problems in

* Now at Institut für Kernphysik Kernforschungszentrum und Universität Karlsruhe, FRG.

determining the effective $\int B\,dl$ value. These facts limit energy determinations to values of typically a few 10^{-4}.

Since improvements in the alternative methods appear to be rather difficult, we have performed a new ultra-high precision energy measurement with the cyclotron time-of-flight spectrometer. To our knowledge the new modified system presently provides the highest energy resolution and the best absolute energy calibration for this kind of work.

In this paper basic aspects of the time-of-flight method are discussed in section 2. The time-of-flight apparatus is described in section 3. Length and time measurements including accuracy estimates are presented in sections 4 and 5. The effective energy resolution function is discussed in section 6. The direct empirical determination of neutron reference peak energies is described in section 7. The formalism used in the resonance analysis is outlined in section 8. The results of the present work are presented and discussed in section 9.

2. General aspects of the time-of-flight method

Energy determinations by the time-of-flight method are, in principle, straight-forward and provide a high potential for precise energy determinations even in the many MeV region.

The kinetic energy of relativistic neutrons can be expressed in terms of flight times t needed to traverse a given flight path of length L:

$$E_n = m_0 c^2 \{[1-(L/ct)^2]^{-1/2} - 1\} \quad (1)$$

where m_0 is the neutron rest mass and c is the light velocity.

The total relative error in energy $\Delta E/E$ results from eq. (1) by adding the squared errors of the different observables:

$$\Delta E/E = 2[(\Delta L/L)^2 + (\Delta t/t)^2 + (\Delta m/2m)^2]^{1/2} \quad (2)$$

with ΔL and Δt being the total uncertainties in length and time, respectively.

Since the neutron mass is known to an accuracy of $\Delta m/m = 5\times10^{-6}$, ref. 4, precise energy measurements depend mainly on accurate length and time determinations. In the MeV region the crucial difficulty is that neutron velocities are close to the velocity of light. Between 3 and 30 MeV neutron velocities range between 2.5 and 7.5×10^9 cm s^{-1}. For reasons concerning intensity flight paths of only a few hundred meters (typically 200 m) can be employed. Therefore, any high precision energy determination must aim at total accuracies of less than 1 mm for length and less than 1 ns for time measurements. Although present techniques allow, in principle, relative length measurements of up to $\Delta L/L = 1\times10^{-6}$ and time determinations of $\Delta t/t \sim 1\times10^{-8}$ (assuming direct conversion of time into frequency information), previous results have been often severely affected by large systematic uncertainties, e.g., those mentioned in the previous section.

3. Experimental set-up

Neutron resonance energies were measured in a standard transmission experiment employing the neutron time-of-flight spectrometer at the Karlsruhe isochronous cyclotron[5]). Fig. 1 shows a simplified schematic drawing of the new time-of-flight set-up. Bombardment of a 3 mm thick natural uranium target with about 50 MeV deuterons provided a time averaged beam current of $\sim 10\,\mu$A, equivalent to a source strength of 1×10^{13} neutrons s^{-1} sr^{-1} in the forward direction. Narrow and intense neutron bursts are produced by simultaneously deflecting 50 microstructure pulses onto the uranium target. Particular effort was made to obtain optimum timing and resolution conditions. Thus, a reduction of the resolution width by almost an additional factor of 3 was obtained mainly by restriction of the deuteron acceptance angle in the centre of the cyclotron. Neutron bursts of partially less than 0.7 ns duration (fwhm) were produced at a repetition rate of 50 kHz by means of a particular deflection-bunching system described elsewhere[6]). To achieve the necessary long-term stability of optimum cyclotron conditions, the new computer-controlled beam diagnostic system CICERO[7]) was employed for measurements and readjustments of phase unisochronisms and deuteron beam mismatchings.

A narrow neutron beam of 1×10^{-7} sr at an angle of 0° to the incident deuterons was obtained by three collimators positioned along the flight path. Neutrons are detected at the end of an evacuated flight tube. The neutron detector was a small cylindrical NE 102 A plastic scintillator of 5 cm diameter and 1.2 cm length mounted on a Valvo 56 AVP photomultiplier. The photomultiplier tube was selected specifically with respect to optimum time characteristics. Its time resolution for gamma-rays from a ^{60}Co source was determined to be 290 ps. Fast timing of the neutron detector was accomplished by the constant fraction method. Time-of-flight measurements were performed with a digital

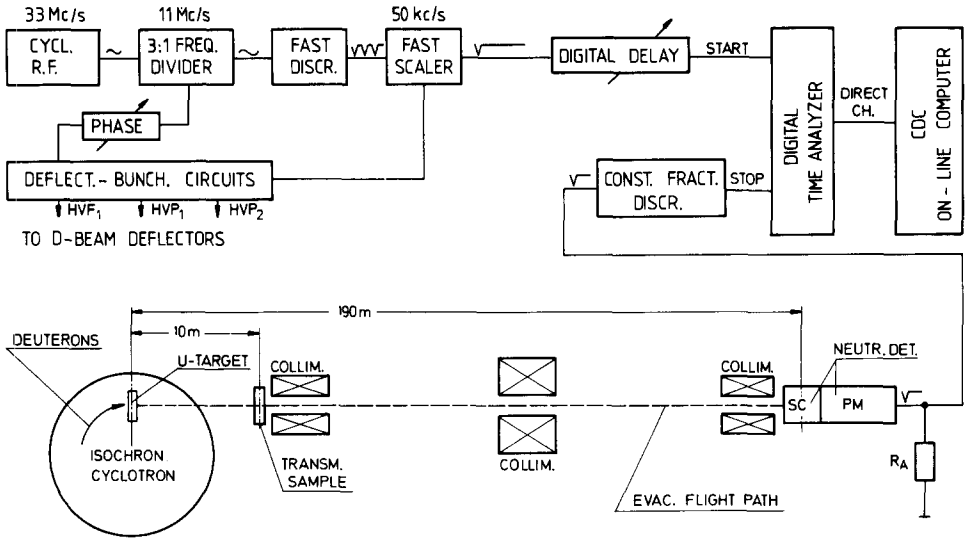

Fig. 1. Schematic drawing of the time-of-flight arrangement. For clarity details of the deflection-bunching system and the complete set of logic circuits are not shown.

time analyzer, employing 28672 channels of 250 ps channel width. For time recording the fast constant fraction discriminator pulse served as the timing reference at the stop input of the time analyzer, whereas the start input was derived from the cyclotron rf. The output of the digital time analyzer was connected to the direct input channel of a modified CDC-3100 on-line computer. Data transfer to the core memory of the computer involved two fast four-word buffers.

Transmission samples are mounted on a remotely-controlled sample changer placed at a distance of 10 m from the neutron source. The carbon sample consisted of a brick of pyrolytic graphite having a thickness of 1.019 atoms b^{-1}. The chemical purity of the material was 99.993%. In the carbon experiment the transmission sample was periodically removed from the beam, typically in a 5 min cycle. For oxygen a liquid sample of 99.91% chemical purity was used. The liquid oxygen was irradiated in a large Dewar sphere of nearly 28 cm diameter. The empty Dewar transmission spectrum was measured in addition for background compensation. Using only a narrow neutron beam passing the centre of the Dewar vessel an effective average sample thickness of 1.201 atoms b^{-1} was derived. The large sample thicknesses in both measurements were chosen in order to also obtain a high sensitivity for weak resonances with small resonance excursions typical for neutron resonances in the many MeV region.

In the range from 3–15 MeV open beam and sample transmission spectra were measured with a typical statistical accuracy ranging between 0.3–1%. The calculation of total cross sections required small corrections for background effects and dead-time losses. Corrections for multiple scattering turned out to be negligible. Typical background corrections were of the order of 1–3%, while dead-time losses did not exceed 0.1%. Due to possible long term effects in the oxygen run, where the transmission and the background spectra were measured at different times, the total cross section curve was normalized at 3.5 MeV to our previous thin sample measurement[6]).

4. Flight path length measurement

As shown in fig. 2 the total flight path length results from the five partial distances

$$L = L' + \sum_{i=1}^{4} l_i, \tag{3}$$

where L' is the distance between the backsurface of the neutron target and the reference point B′ near the detector, 2.5 m above ground level; l_1 means the average distance traversed by the neutrons in the target, l_2 the length between the reference point B′ and the detector surface; l_3 and l_4 are the thickness of the scintillator cap and half of the scintillator length, respectively. Using an electro-optical method the gross distance between A and B′ was determined to be $L' = (18630.95 \pm 0.07)$ cm. This measurement was performed by the "Geodätisches Institut" of the Karlsruhe University employing a

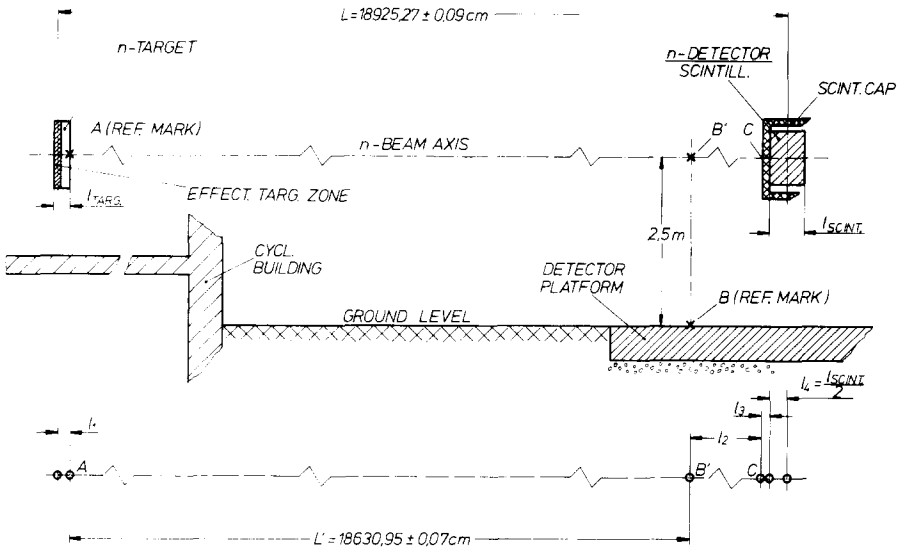

Fig. 2. Principle of the flight path length measurement. The gross distance L' was measured along the n-beam axis by an electro-optical method. For the total length an overall accuracy of $\Delta L/L = 4.6 \times 10^{-6}$ was achieved.

NPL Hilger Mekometer, ME 3000 [8]). The Mekometer ME 3000 is a high precision instrument designed particularly for measurements in the range from 100–3000 m. It employs a pulsed light beam from a xenon source whose polarization is modulated at 500 Mc s^{-1} by means of a potassium dihydrogen phosphate (PDP) light modulator. On return from a distant target reflector the light is demodulated in the same apparatus. Length determination is accomplished by phase comparison of the transmitted and the received modulation. The ME 3000 System is equipped with an automatic compensation for atmospheric changes of the refractive index[9]). An overall accuracy of less than 0.2 mm is guaranteed by the manufacturer for phase determinations with this type of instrument. The given accuracy for the value of L', which is more than three times larger than the above value, resulted from statistical errors of several independent measurements at different times.

The reference mark B defining the interception of L' and l_2 is fixed on a large detector platform of 6×10 m^2 well founded in the soil. Although the other endpoint of L' lies on the reverse side of the moveable neutron target, its irradiation position can be reproduced with high accuracy in the cyclotron internal coordinates. From several measurements during the last few years it was proven that the target centre position was reproduceable in all three space coordinates by better than 0.2 mm provided accurate mounting of the target and precise adjustment of the target support are made. An estimate of the soil stability around the cyclotron building by the "Geodätisches Institut" gave an upper limit of 0.3 mm for a long-term variation in L'. The distance l_2 was measured by a precision meter calibrated by the PTB Braunschweig to be (292.90 ± 0.05) cm. Finally, the scintillator thickness including the length of the Al scintillator cap and the neutron target thickness l_{TARG} were determined by use of standard micrometers. These measurements gave $l_3 + l_4 = (0.65 \pm 0.01)$ cm and $l_{TARG} = (0.80 \pm 0.01)$ cm.

In order to fix the last required quantity l_1, the average path of neutrons in the target, we have to consider the details of neutron production. As indicated by Schweimer[10]) and verified by own results more than 80% of neutrons produced in the bombardment of thick natural uranium targets with 52 MeV deuteron originate from high energy deuterons having an energy higher than 40 MeV. For uranium a 12 MeV energy loss of 52 MeV deuterons corresponds to a penetration depth of ~ 0.06 cm. Assuming a linearly decreasing source strength the average lengths l_1 was determined to be (0.77 ± 0.01) cm. This figure would only change by 0.007 cm even for a most improbable exponential intensity–depth relation.

On this basis the total flight path length becomes

$$L = L' + l_1 + l_2 + l_3 + l_4 = (18925.27 \pm 0.09)\ \text{cm}.$$

The above stated error also includes systematic errors due to incorrect adjustments of the target and detector surfaces perpendicular to the neutron beam axis. As a matter of fact an accuracy of the absolute length determination of $\Delta L/L = 4.6 \times \times 10^{-6}$ was achieved in the present experiment.

5. Time-of-flight measurements

Neutron flight times are measured by a digital time analyzer developed by LABEN, Italy[11]). The actual system (LABEN UC-KB) has a maximum capacity of 262 144 channels of 250 ps channel width. The operation principle is based on a continuously running clock and time readings are made by the sampling of a suitable number of synchronously running oscillators of frequencies between ~ 250 MHz and ~ 15 kHz, changing in steps of a factor two. These oscillators are tuned by a highly stabilized master clock quartz oscillator having a frequency $f_{mc} = (7\,812\,339.2 \pm 0.2)$ Hz. Above 500 MHz additional 3 bits are produced by a digital interpolation system of 8 oscillators all running at the maximum frequency, but with precisely adjusted delays staggered at 250 ps intervals. With this system an overall differential linearity of better than 0.2% is achieved. From the description it is evident that the task of a flight time measurement reduces to that of a frequency determination of the master clock which is calibrated and stabilized to 2.5×10^{-8}.

For an absolute flight time measurement an accurate time-zero point is also necessary. This reference point was provided by the peak of prompt gamma-rays produced during the deuteron bombardment of the neutron target. Prompt gamma-rays arrive at the detector at a time $T_\gamma = L/c$ after neutron production. Experiencing a symmetric gamma-peak distribution, the exact peak position was determined by the cumulative probability method[1]) with an accuracy of ± 25 ps ($\frac{1}{10}$ of the channel width). Time spreads due to the finite target and detector thicknesses for γ-rays are small compared with the total time-averaged pulse width of ~ 950 ps. The respective transit times are 3.3 ps for the neutron source and 43 ps for the scintillator. Having a precise time-zero-reference, any accurate energy determination depends on the measurement of precise peak positions of sufficiently narrow neutron resonances.

6. Experimental resolution function

Experimentally, five components contribute to the total resolution function:

(i) the neutron burst distribution,
(ii) the detector resolution function characterized by the detector jitter,
(iii) the time spread introduced by the finite length of the source,
(iv) the time uncertainty produced by the thickness of the scintillator and
(v) the Doppler effect.

From these only the first two quantities are independent of the neutron energy. Fortunately, however, these are the most important components of the total resolution function.

The detector resolution function has been measured in an auxiliary run, employing two identical n-detectors and a ^{60}Co-gamma source. From this measurement a Gaussian distribution of (290 ± 10) ps (fwhm) was derived for a single detector. This result is also representative of neutron detection in the range from 3–10 MeV, because of the similar dynamical range (due to the, by an order of magnitude higher, light output for γ-rays) and the almost similar shapes of the spectra. Moreover, it could be shown, that the resolution width changed by less than 50 ps when the dynamic range was increased or reduced by a factor of two.

The knowledge of the detector resolution function in turn allows the neutron burst distribution from the measured prompt gamma-peak to be determined by a simple unfolding procedure. This is possible, since for gamma-rays the two components (iii) and (iv) are negligible (cf., section 5), and thus the gamma-peak reflects only the effects (i) and (ii). From unfolding an almost Gaussian resolution function of 950 ps (fwhm) was obtained.

The time spread introduced by the source extension is also small for neutrons in the range investigated from 3–30 MeV. As discussed in the previous section almost all neutrons are produced in a surface region of ~ 0.6 mm thickness. The corresponding time spread of fast neutrons is 25 and 8 ps for 3 and 30 MeV neutrons, respectively, which can be neglected.

The effect from contribution (iv) is more than an order of magnitude higher. Neutron transit times through the 1.2 cm thick proton recoil scintillator range between 160–500 ps, introducing in a zeroth order guess a rectangular time distribution. In detail, however, neutron attenuation in the scintillator has to be taken into account the effect of which

might sometimes cause significant deviations from a rectangular shape. In the present case attenuation effects were small (typically between 2–5%). Therefore, the use of a rectangular shape did not introduce significant changes in the total resolution function.

At the high resolution obtained in this work Doppler-broadening has also to be taken into account. For this purpose the velocity distribution of the sample nuclei along the neutron beam axis is needed. The distribution results from the average energy per vibrational degree of freedom. In the case of a solid or a liquid sample the classical mean energy kT ought to be replaced by the quantal mean energy $\bar{\varepsilon}$ of the oscillation modes including the zero-point energy

$$\bar{\varepsilon} = 1/2 \int_0^{\nu_{max}} h\nu \coth(h\nu) g(\nu) \, d\nu, \quad (4)$$

where $g(\nu)$ is the normalized spectrum of oscillation modes in the sample and ν_{max} is the maximum frequency.

Inserting for carbon the room temperature $T = 298$ K and using phonon spectra of graphite from the literature[12,13]) an average value of (60.0 ± 4) meV was determined. This allowed in turn the Doppler-width to be calculated from a Gaussian distribution by

$$\Delta = 4[\ln 2 (m/M) \bar{\varepsilon} E]^{1/2} \quad (5)$$

where Δ refers to the fwhm width in the laboratory system, m and M are neutron and target mass and E is the neutron energy in the laboratory system. For oxygen we estimated a mean energy $\bar{\varepsilon} = (47.8 \pm 1.0)$ meV which is determined by the strong zero-point oscillation energy of the O_2 molecules. The various contributions to the total effective resolution function are summarized in table 1.

TABLE 1

Contributions to the effective resolution function. Details of experimental determinations and calculations are described in the text.

Contribution	Shape	$\Delta t/t \times 10^4$ 30 MeV	3 MeV
Deuteron beam spread	Gaussian-like	3.7	1.2 fwhm
Detector jitter	Gaussian	1.1	0.37 fwhm
Detector thickness	Rectangular	0.63	
Doppler broadening	Gaussian	0.22[a]	0.68[a] fwhm
Effective Gaussian-like resolution		3.9	1.6 fwhm

[a] Calculated for the graphite sample.

The effective resolution for the final resonance analysis (see section 8) was obtained by folding the measured time spectrum of the prompt γ-peak, the Gaussian Doppler broadening and the rectangular time spread introduced by the neutron transit times in the neutron detector.

7. Direct determination of reference peak energies

Neutron resonance energies can, in principle, be directly obtained from measured peak positions of symmetric resonances. However, in the MeV region not only s-wave, but also resonances of higher partial waves occassionally exhibit marked asymmetries caused by resonance–potential interference. Even though peak and resonance energies do not coincide any more in this case, peak energies are still useful for reference purposes, as long as resolution effects are negligible. Their use in auxiliary calibration experiments is even more convenient, since it exempts one from performing time-consuming resonance analyses. The situation is more complex when significant resolution broadening occurs. Especially for strongly asymmetric resonances with pronounced interference minima observed peaks are increasingly displaced from the unperturbed positions with increasing resolution broadening. This effect requires suitable corrections.

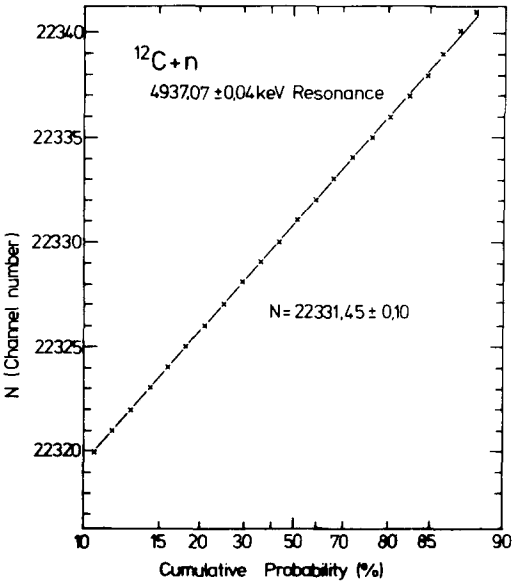

Fig. 3. Cumulative probability distribution for the 4937 keV resonance in ^{12}C+n. The straight line is the result of a least squares fit to the data between 10 and 90% probability. This method allowed the derivation of the peak position with an accuracy of 0.10 time channels.

A pragmatic solution in this case is to provide unperturbed positions of both, resonance peaks and interference minima, as the reference information. These are, in principle, sufficient to correct any given measurement for individual resolution effects. A more general description of all resonances is, nevertheless, given by a set of resonance parameters obtained from detailed resonance analyses (see section 8).

When the observed shape of a resonance is symmetric and mainly Lorentzian or Gaussian (if resolution broadening is predominant) the accuracy in deducing the position of a resonance peak can considerably be improved by the use of a cumulative probability plot. For this purpose a suitable background representing the neighbouring cross section data (mainly a weakly energy dependent background) has to be subtracted. The resonance cross section data points are then treated as probability values and plotted on probability graph paper against timing channel number. The linear part of the curve can be taken to derive the timing channel corresponding to the centre at 50% probability. This technique readily allows peak positions with an accuracy of 0.1 channels or less to be estimated. An example of this treatment is shown in fig. 3 which illustrates the results of a Lorentzian probability display for the 4937.07 keV resonance of $^{12}C+n$. Half a channel must be added to the derived 50% probability value, because of the binning into discrete channels. The straight line was obtained from a least squares fitting of the data between 10 and 90% probability. Derived errors also reflect the observed departure from a pure Lorentzian.

A modified treatment was applied for the slightly asymmetric resonances at 4.527 and 5.369 MeV in oxygen and at 5.368 MeV in carbon. In order to obtain a nearly symmetric distribution, the same number of data points at both sides of the measured peak channel were selected for analysis. A total range of two times the difference between the peak and the interference minimum positions was chosen. A reasonable background to be subtracted is defined by the straight line representing the data at both ends of the selected range. Finally, suitable corrections were made for missed probabilities outside the analyzed region. It turned out from auxiliary computer calculations that this method provides peak positions with an accuracy of better than 0.4 channels considering asymmetries and widths within the range of the present work.

Peak positions of the three broad resonances at 6.820 and 7.199 MeV in oxygen and at 7.726 MeV in carbon were taken directly from the cross section curves using a nine channel sliding average.

8. Resonance analyses

Besides the direct determination of cross section peak energies (see section 7) isolated resonance excursions in the systems $^{12}C+n$ and $^{16}O+n$ were analyzed assuming non-interfering multi-level Breit–Wigner resonances[14]). This seemed reasonable, since the interference with broad resonances mainly alters the phase between the narrow resonance amplitude and the weakly energy dependent background amplitude, i.e., the interference pattern of the resonance shape. It leaves, however, the important parameters E_R as well as the total width Γ practically unchanged. Thus, any broad resonance amplitude can be treated as part of a smoothly energy dependent background amplitude. In this formalism the complex scattering matrix element S_{LJ} for a resonance channel with orbital angular momentum L and total angular momentum J can be expressed by[15])

$$S_{LJ} = S_{LJ}^{nr} - i\Gamma_{n_0}/(E-E_R+i\Gamma/2) \times \times \exp[2i(\mathrm{Re}\,\delta_{LJ}^{nr}+\phi_{LJ}^{r})], \quad (6)$$

where S_{LJ}^{nr} is the smoothly energy dependent background amplitude, Γ_{n_0} the groundstate neutron decay width and E_R the neutron resonance energy. Γ means the total width, $\mathrm{Re}\delta_{LJ}$ the real part of the background phase shift and ϕ_{LJ} a possible resonance phase. It should be noted that the resulting resonance parameters are directly related to the complex poles of the S-matrix. The one-to-one correspondance to the R-matrix parametrization is only valid in the extreme single level limit.

Employing the usual relation for the total cross section

$$\sigma_t = \frac{2\pi}{k^2}\sum_{lj}(j+\tfrac{1}{2})\,\mathrm{Re}(1-S_{lj}), \quad (7)$$

where k means the cm neutron wave number, it is possible to separate this expression for the total cross section into a non-resonant background term σ_t^{nr} and a purely resonant term (or a sum of resonant terms, if more than one level is involved)

$$\sigma_t = \sigma_t^{nr} + \frac{\pi}{k^2}(J+\tfrac{1}{2})\Gamma_{n_0}/[(E-E_R)^2+(\Gamma/2)^2] \times \times \{2(E-E_R)\cos 2\varphi + \Gamma \sin 2\varphi\}, \quad (8)$$

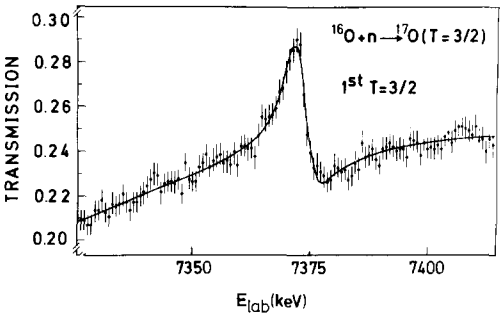

Fig. 4. Resonance excursion of the first $T=\frac{3}{2}$ resonance in ^{17}O. The solid line was obtained from a single-level Breit–Wigner analysis of the transmission data.

using the identity $\varphi = \mathrm{Re}\delta_{LJ}^{nr} + \phi_{LJ}^{r} + \pi/4$. The quantities E, E_R, Γ and Γ_{n_0} are related either to the laboratory system or to the cm system.

Finally, instead of the total cross section σ_t the transmission T is directly fitted using the experimentally known sample thickness ρ in units of atoms/barn

$$T = \exp(-\rho\sigma_t). \tag{9}$$

For numerical calculations the slowly energy dependent term σ_t^{nr} is parametrized by the usual quadratic form[16])

$$\sigma_t^{nr} = a + b(E-E_R) + c(E-E_R)^2. \tag{10}$$

This parametrization makes it possible to determine the essential resonance parameters E_R, Γ and Γ_{n_0} (or $(J+\frac{1}{2})\cdot\Gamma_{n_0}$ if J is not known) without any detailed specification of the background amplitudes. Including the phase φ as a single fit parameter the following seven parameters were adjusted to the experimental data: a, b, c, φ, E_R, Γ and Γ_{n_0}. The correlation between the fit parameters is weak. Therefore, the resonance parameters can be determined with high precision using a least-squares fitting procedure. A correct statistical error assignment is obtained using the standard error matrix which includes the correlation between fit parameters. The final error is obtained by adding quadratically the statistical error and the absolute calibration errors.

Theoretical excitation functions according to eq. (9) were folded by the total effective resolution function before applying an automatic least squares fitting routine[17]). A typical example of a resonance fit with this method is shown in fig. 4. It can be seen that the theoretical curve gives an excellent fit of the experimentally observed $T=\frac{3}{2}$ resonance excursion at $E_R = 7373$ keV.

9. Results

In figs. 5 and 6 total neutron cross sections of carbon and oxygen are shown in the range from 4.5–8.0 MeV which may serve as a typical example of the present high quality results. Numerical values of the complete set of 28K data points for each element in the range from 3–30 MeV can be obtained on request from the NEA Data Bank*. It can be seen that the systems $^{12}C+n$ and $^{16}O+n$ exhibit a simple resonance structure with a number of extremely narrow resonances suitable for standard purposes in ultra-high resolution investigations. In addition several slightly broader resonances of mostly symmetric shape are observed which can be used for normalization in less resolved experiments failing to resolve the narrowest resonances. Three additional resonances below 4.5 MeV in ^{17}O are shown in fig. 7. Especially the double peak near 3440 keV demonstrates the high resolution power of the present set-up. The $J^\pi = (\frac{5}{2}^+)$ resonance at 3438.60 keV and the $J^\pi = \frac{5}{2}^-$ resonance at 3441.63 keV are well resolved.

9.1. Neutron reference peak energies

Obviously the quality of a reference energy determination depends primarily on the quantity Γ/E_n which has thus been recently adopted as a measure for standard energy classifications[1]). Moreover, for

* NEA Data Bank, PO Box 9, F-91190 Gif-sur-Yvette, France.

TABLE 2

Category I resonances of $^{16}O+n$ and $^{12}C+n$ suggested as energy standards for ultra-high resolution measurements (peak energies E_n and widths Γ in the laboratory system). For resonance classification see text.

E_n (keV) [b]	Γ(keV) [b]	Γ/E_n	$\Delta E/E$ [c]
	Oxygen		
3211.68±0.04	1.4 ±0.1	4.4×10^{-4}	1.2×10^{-5}
3438.60±0.06 [a, d]	0.58±0.15 [d]	1.7×10^{-4}	1.7×10^{-5}
3441.63±0.04 [d]	0.84±0.10 [d]	2.4×10^{-4}	1.2×10^{-5}
4594.83±0.07	1.9 ±0.15	4.1×10^{-4}	1.5×10^{-5}
5369.51±0.11 [a]	3.4 ±0.2	6.3×10^{-4}	2.0×10^{-5}
6076.19±0.11	4.1 ±0.2	6.7×10^{-4}	1.8×10^{-5}
	Carbon		
4937.07±0.07	2.1 ±0.15	5.5×10^{-4}	1.4×10^{-5}

[a] Asymmetric resonance shape.
[b] Derived from a Lorentzian probability plot unless otherwise noted.
[c] Calculated from eq. (2).
[d] Derived from a Gaussian probability plot.

energy standards it is convenient to use peak energies rather than resonance energies, since they are immediately observed in auxiliary transmission experiments proposed for energy calibrations. On this basis we have produced two tables of neutron standard energies separating the narrow resonances in carbon and oxygen into two categories according to their respective Γ/E_n values. While table 2 lists the resonances having values of $\Gamma/E_n < 1 \times 10^{-3}$ suitable for ultra-high resolution experiments (category I), table 3 contains resonances in the range $10^{-3} \leq \Gamma/E_n \leq 10^{-2}$ (category II) which may be the only narrow ones observed with usual high-resolution neutron spectrometers. Errors given for peak energies in column 1 are overall uncertainties calculated from eq. (2). Widths in column 2 concern

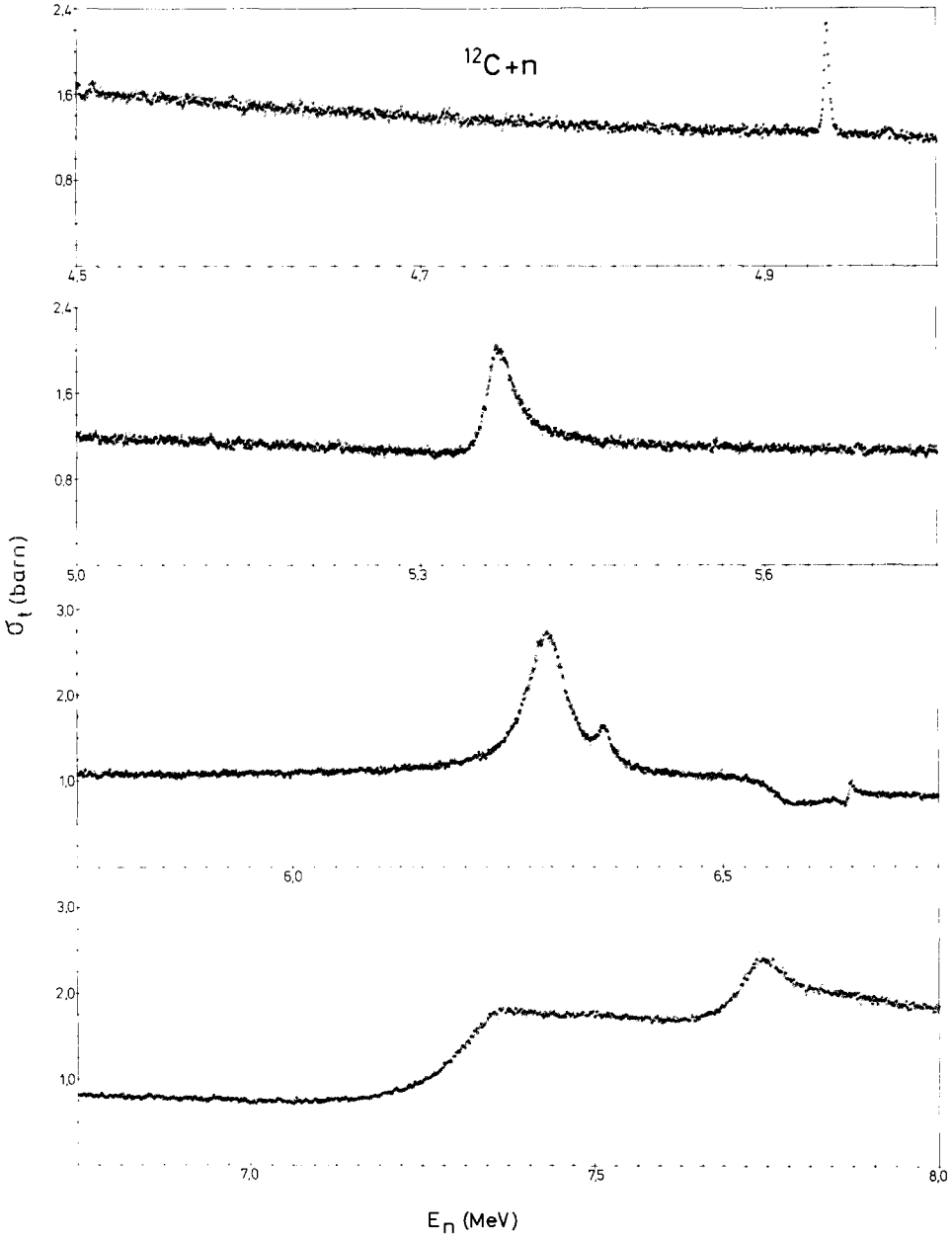

Fig. 5. Total neutron cross section of carbon between 4.5–8 MeV. Numerical values of the whole set of 28 K data points measured between 3–30 MeV can be obtained on request from the NEA Data Bank.

fwhm derived from cumulative probabilities between 25 and 75% for not or only weakly resolution-broadened resonances (Lorentzian shape) and cumulative probabilities between 11 and 89% for strongly resolution-broadened resonances (Gaussian shape). The values given have been corrected for resolution effects where necessary. The third and the last columns contain the actual Γ/E_n-values and the total relative uncertainties $\Delta E/E$, respectively.

Although less suitable for energy calibrations than symmetric resonances, table 4 lists the results for two narrow, but strongly asymmetric resonances for completeness. In this case experimental information concerns the resolution-corrected energies of resonance peak and interference minimum posi-

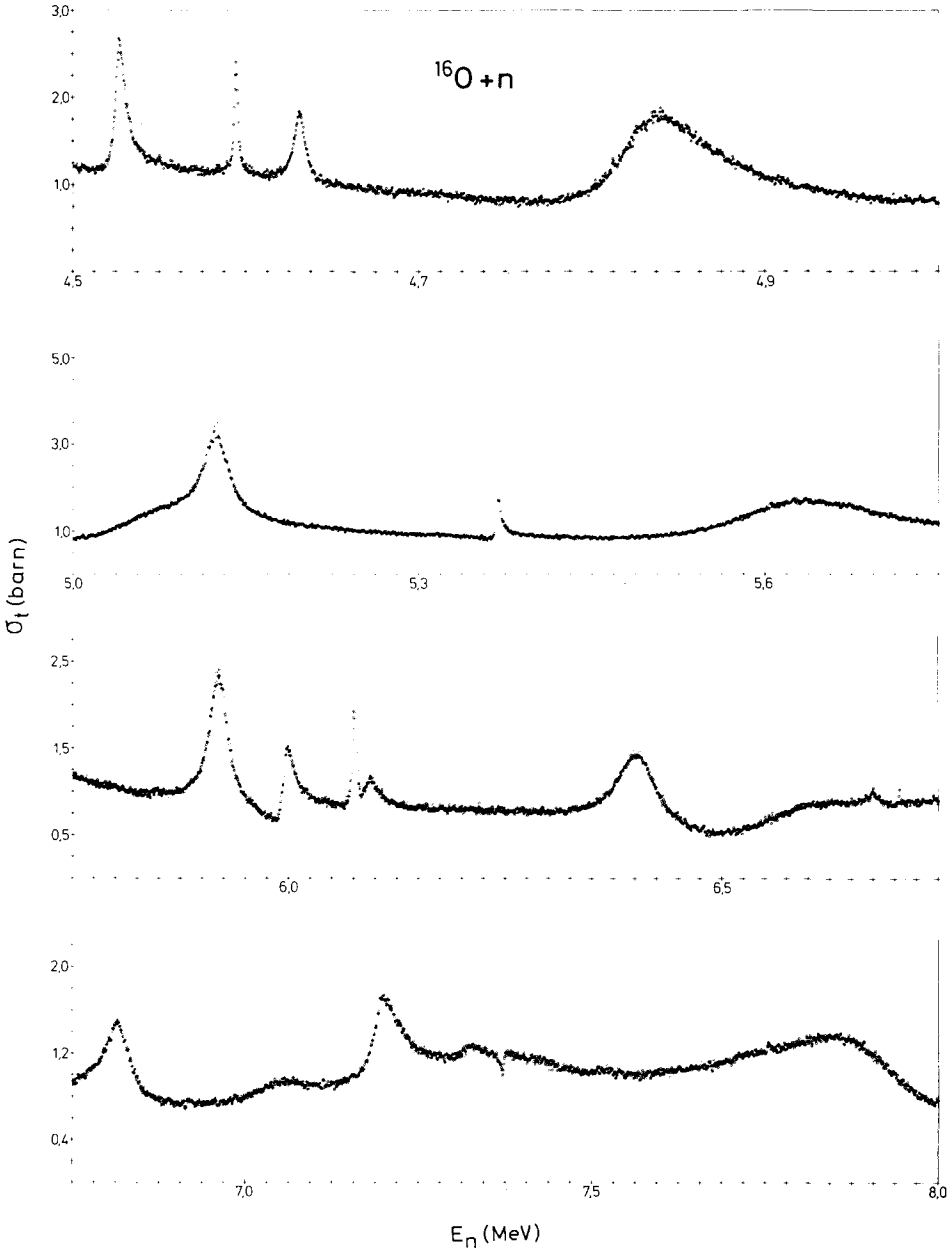

Fig. 6. Total neutron cross section of oxygen in the range from 4.5–8 MeV. These data illustrate the high quality of the present experimental results.

TABLE 3

Category II resonances of $^{16}O+n$ and $^{12}C+n$ proposed as energy standards in usual high-resolution experiments (peak energies E_n and widths Γ in the lab system).

E_n (keV)[b]	Γ (keV)[b]	Γ/E_n	$\Delta E/E$[c]
	Oxygen		
3767.57±0.15	15.1±0.3	4.0×10^{-3}	4.0×10^{-5}
4527.60±0.20[a]	6.2±0.2	1.4×10^{-3}	4.4×10^{-5}
4631.57±0.13	6.8±0.3	1.5×10^{-3}	2.8×10^{-5}
5124.55±0.25	25.3±2.1	4.9×10^{-3}	4.9×10^{-5}
5919.72±0.25	24.3±2.2	4.1×10^{-3}	4.2×10^{-5}
6094.38±0.36	19.4±2.2	3.2×10^{-3}	4.3×10^{-5}
6401.41±0.40	50.6±2.5	7.9×10^{-3}	6.2×10^{-5}
6816.86±0.65[a, d]	44.2±2.5[d]	6.4×10^{-3}	9.5×10^{-5}
7204.55±0.71[a, d]	42.7±3.0[d]	5.9×10^{-3}	9.9×10^{-5}
	Carbon		
5368.12±0.30[a]	23.7±4.0	4.4×10^{-3}	5.6×10^{-5}
6296.82±0.39	53.8±1.2	8.5×10^{-3}	6.2×10^{-5}
6361.43±0.38	19.3±1.2	3.0×10^{-3}	6.0×10^{-5}
7746.95±0.63[a, d]	71.2±6.5[d]	9.3×10^{-3}	8.1×10^{-5}

[a] Asymmetric resonance shape.
[b] Derived from a Lorentzian probability plot unless otherwise noted.
[c] Calculated from eq. (2).
[d] Obtained directly from cross section curves (see text).

tions, which both are necessary to derive E_n directly from an experiment of given spectrometer resolution[18]). Instead of the width the energy difference E_n-E_m was taken in the fourth line for resonance classification.

9.2. Neutron resonance energies from the resonance analysis

Resonance parameters obtained from the analysis described in section 8 are listed in tables 5a and b. Resonance energies and widths are given for the laboratory system as well as the cm system. Column 4 contains the phase parameter φ [see eq. (8)] which is a measure of the interference shape asymmetry of the resonance. A symmetrical Lorentzian peak in σ_{tot} corresponds to $\varphi=45°$. Resonance energies and widths deviate from the respective values in tables 2 and 3 mainly because of the shape asymmetry effects. Spin and parity assignments are taken from refs.[19,20]). In cases of unknown J^π values a possible J^π value has been assumed for computing a possible partial width Γ_{n_0}.

Since the shape asymmetry effects are precisely taken into account by the fit parameter φ the values in tables 5a and b are recommended not only for

TABLE 4

Experimental results of two narrow, but strongly asymmetric $T=\frac{1}{2}$ resonances of $^{16}O+n$ and $^{12}C+n$. Although less suitable as energy standards than symmetric resonances these data are given for completeness.

Quantity	$^{16}O+n$ 5995.68 keV Resonance	$^{12}C+n$ 6646.71 keV Resonance
Peak energy E_n (keV)	5999.10±0.53[a]	6648.41±0.32[a]
Interf. minimum Energy E_m (keV)	5987.25±0.53[a]	6642.75±0.32[a]
Energy difference E_n-E_m (keV)	11.85±0.75	5.66±0.45
$\frac{E_n-E_m}{E_n}$	19.8×10^{-4}	8.5×10^{-4}
$\Delta E/E$	8.8×10^{-5}	4.8×10^{-5}

[a] Corrected for resolution broadening.

neutron resonance energy calibrations but also for charged particle resonance energy calibrations using the corresponding $^9Be+\alpha$ and $^{13}C+\alpha$ resonances.

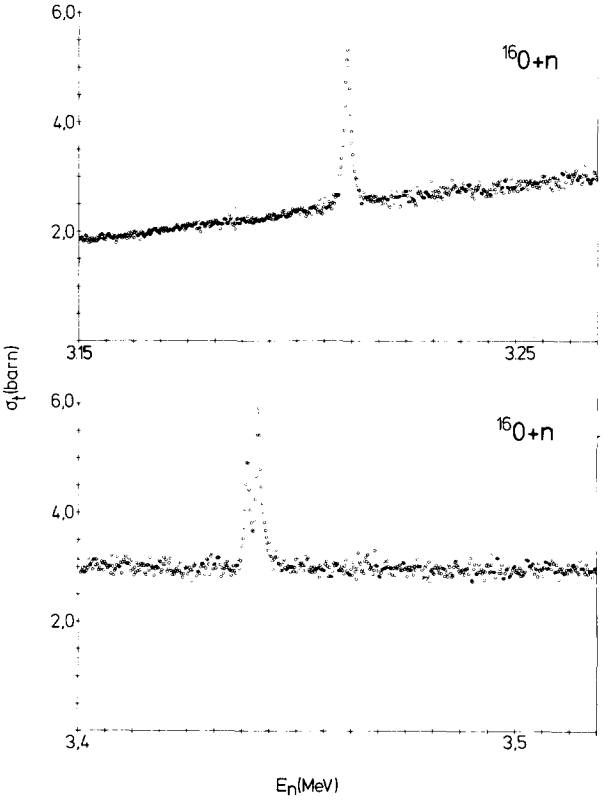

Fig. 7. Total cross section of oxygen in the vicinity of three narrow resonances near 3.2 and 3.4 MeV. With the high resolution of the Karlsruhe spectrometer the $J^\pi=(\frac{5}{2}^+)$ at 3438.60 keV and the $J^\pi=\frac{5}{2}^-$ resonance at 3441.63 keV are well resolved.

TABLE 5a

$^{16}O + n$ resonance parameters from the resonance analysis and recommended ^{17}O excitation energies.

Lab. system				cm system				
E_R (keV)	Γ (keV)	Γ_{n_0} (keV)	φ (deg.)	E_R (keV)	Γ (keV)	Γ_{n_0} (keV)	E_x (keV)[a]	J^π [b]
3211.70±0.17	1.45±0.05	1.45±0.05	45.0±1.3	3020.89±0.16	1.38±0.05	1.38±0.05	7165.19±0.8	$\frac{5}{2}^-$
3438.38±0.19	0.68±0.24	0.68±0.24	28.1±5.7	3243.08±0.19	0.64±0.23	0.64±0.23	7378.38±0.8	$\frac{5}{2}^+$
3441.73±0.14	1.02±0.21	1.02±0.21	48.2±4.2	3237.23±0.14	0.96±0.20	0.96±0.20	7381.53±0.8	$\frac{5}{2}^-$
3767.76±0.22	15.4 ±0.3	13.8 ±0.6	48.3±1.4	3543.86±0.21	14.4 ±0.3	13.0 ±0.6	7688.16±0.8	$\frac{7}{2}^-$
4463.41±0.26	12.1 ±0.5	8.6 ±0.3	93.6±2.6	4198.08±0.24	11.4 ±0.5	8.1 ±0.3	8342.38±0.8	$\frac{1}{2}^+$
4527.12±0.07	6.56±0.14	5.05±0.12	35.0±0.4	4258.00±0.07	6.17±0.13	4.75±0.11	8402.30±0.8	$\frac{5}{2}^+$
4594.83±0.09	2.26±0.12	1.25±0.04	45.1±1.0	4321.67±0.09	2.13±0.11	1.18±0.04	8465.97±0.8	$\frac{7}{2}^+$
4631.78±0.12	7.33±0.23	3.04±0.09	48.4±0.8	4356.38±0.11	6.89±0.22	2.86±0.08	8500.68±0.8	$\frac{5}{2}^-$
4829.9 ±0.4	58.8 ±0.6	52.0 ±1.2	26.1±1.0	4542.7 ±0.4	55.3 ±0.6	48.9 ±1.1	8687.0 ±0.9	$\frac{3}{2}^-$
5127.0 ±1.6	28.0 ±2.0	25.0 ±2.0	50.0±3.0	4822.1 ±1.5	26.3 ±1.9	23.5 ±1.9	8966.4 ±1.7	$\frac{7}{2}^-$
5368.90±0.09	3.75±0.14	2.52±0.08	30.4±0.7	5049.61±0.08	3.53±0.13	2.37±0.08	9193.91±0.8	$\frac{5}{2}^+$
5919.67±0.14	24.6 ±0.3	19.1 ±0.6	46.6±0.3	5567.53±0.13	23.1 ±0.3	18.0 ±0.6	9711.83±0.8	$\frac{7}{2}^+$
5995.68±0.15	12.4 ±0.3	10.9 ±0.3	19.4±0.6	5639.00±0.14	11.7 ±0.3	10.3 ±0.3	9783.30±0.8	$\frac{3}{2}^+$
6076.08±0.15	4.26±0.24	3.58±0.21	45.2±1.4	5714.61±0.14	4.01±0.23	3.37±0.20	9858.91±0.8	$(\frac{5}{2}^-)$[c]
6094.8 ±1.0	17.8 ±1.8	11.6 ±1.3	39.0±3.0	5732.3 ±0.9	16.7 ±1.7	10.9 ±1.2	9876.6 ±1.2	$(\frac{1}{2}^-)$[c]
6404.6 ±0.5	52.2 ±0.8	23.7 ±0.6	50.1±1.3	6023.5 ±0.5	49.1 ±0.8	22.3 ±0.6	10167.8 ±0.9	$(\frac{7}{2}^-)$[c]
6820.7 ±0.6	45.2 ±1.2	18.3 ±0.7	55.7±1.5	6414.8 ±0.6	42.5 ±1.1	17.2 ±0.7	10559.1 ±1.0	$(\frac{7}{2}^-)$[c]
7199.3 ±1.3	44.4 ±1.5	28.1 ±1.0	34.6±1.9	6770.8 ±1.2	41.7 ±1.4	26.4 ±0.9	10915.1 ±1.4	$(\frac{5}{2}^+)$[c]
7373.31±0.18	2.5 ±0.3	2.00±0.13	−22.2±1.8	6934.38±0.17	2.4 ±0.3	1.88±0.12	11078.68±0.8	$\frac{1}{2}^-$
8848.8 ±0.6	7.3 ±1.2	1.35±0.15	68.4±3.6	8321.7 ±0.6	6.9 ±1.1	1.27±0.14	12466.0 ±1.1	$\frac{3}{2}^-$
9414.9 ±0.6	2.7 ±1.1	0.43±0.06	88.6±4.4	8854.0 ±0.6	2.5 ±1.0	0.40±0.06	12998.3 ±1.0	$\frac{5}{2}^-$
10725.5 ±1.5	21.8 ±1.7	2.20±0.17	105.8±2.4	10086.0 ±1.4	20.5 ±1.6	2.07±0.16	14230.3 ±1.6	$\frac{7}{2}^-$

[a] $^{16}O - n$ binding energy $B = (4144.3 \pm 0.8)$ keV from ref. 4.
[b] Ref. 19 unless otherwise noted.
[c] Present work.

TABLE 5b

$^{12}C + n$ resonance parameters from the resonance analysis and recommended ^{13}C excitation energies.

Lab. system				cm system				
E_R (keV)	Γ (keV)	Γ_{n_0} (keV)	φ (deg.)	E_R (keV)	Γ (keV)	Γ_{n_0} (keV)	E_x (keV)[a]	J^π [b]
4937.12±0.09	1.87±0.08	1.72±0.04	44.9±1.6	4553.45±0.09	1.72±0.08	1.60±0.04	9499.84±0.09	$(\frac{5}{2}^-)$[c]
5365.21±0.18	25.7 ±0.4	22.3 ±0.5	31.4±0.4	4948.19±0.17	23.7 ±0.4	20.6 ±0.5	9894.58±0.17	$\frac{3}{2}^-$
6297.07±0.32	55.2 ±0.6	47.0 ±1.0	47.2±0.4	5807.42±0.30	50.9 ±0.6	43.4 ±0.9	10753.8 ±0.3	$\frac{7}{2}^-$
6361.1 ±0.6	19.6 ±1.1	5.1 ±0.3	41.7±1.5	5866.5 ±0.6	18.1 ±1.0	4.7 ±0.3	10813.0 ±0.6	$(\frac{5}{2}^-)$
6646.71±0.20	4.3 ±0.4	2.71±0.17	12.4±1.8	6129.78±0.19	4.0 ±0.4	2.52±0.16	11076.20±0.19	$(\frac{1}{2}^-)$
7726.8 ±2.1	88.3 ±3.6	74.8 ±3.3	23.0±1.8	7125.6 ±2.0	81.5 ±3.3	69.0 ±3.0	12072.0 ±2.0	$(\frac{3}{2}^-)$[c]

[a] $^{12}C + n$ binding energy $B = (4946.392 \pm 0.030)$ keV from ref. 4.
[b] Ref. 20 unless otherwise noted.
[c] Present work.

TABLE 6
List of most prominent ^{17}O ($T=\frac{3}{2}$) resonances between 11 and 115 MeV (cm values).

E_x (keV)[a]	Γ (keV)[a]	E_x (keV)[b]	Γ (keV)[b]	E_x (keV)[c]	E_x (keV)[d]	J^{π} [e]
11078.7±0.8	2.4±0.3	11076±5	5.0±1.1	11082±6	11075±4	$\frac{1}{2}^+$
12466.0±1.1	6.9±1.1	12458±5	8 ±2	12471±5		$\frac{3}{2}^-$
12998.3±1.0	2.5±1.0	12993±6	<3	12994±8		$\frac{5}{2}^-$
14230.3±1.6	20.5±1.3			14219±8		$\frac{7}{2}^+$

[a] Present work.
[b] Ref. 21.
[c] Ref. 22.
[d] Ref. 23.
[e] Ref. 19.

The data in table 5 may also be used as very precise calibration standards for the corresponding excitation energies E_x of the ^{13}C and ^{17}O level scheme.

9.3. $T=\frac{3}{2}$ RESONANCES

Above 7 MeV seven $^{16}O+n\rightarrow{}^{17}O(T=\frac{3}{2})$ resonances were observed in the present work. Also the first $^{12}C+n\rightarrow{}^{13}C(T=\frac{3}{2})$ resonance appears as an extremely weak anomaly. The lowest $T=\frac{3}{2}$ resonances are extremely sharp in the respective energy range since the neutron channel and other possible decay channels are isospin-forbidden. An example of a resonance excursion of the $T=\frac{3}{2}$ type is shown in fig. 4. In table 6 resonance energies and widths of the most prominent $^{16}O+n\rightarrow{}^{17}O$ ($T=\frac{3}{2}$) resonances are compared with results from charged particle reactions[21-23]).

10. Summary

The Karlsruhe neutron time-of-flight-spectrometer when used at its extreme capability provides a good means of determining high precision neutron resonance and compound nucleus excitation energies. The accuracy obtained of 1.2×10^5 is to our knowledge the highest achieved so far in the neutron field. This allocates the system a unique role in providing the necessary standards often needed for normalization purposes and for solving existent discrepancies in energy scales. The present time-of-flight system also opens exciting perspectives for new investigations in basic research. Among others we would like to mention systematic studies of isospin-forbidden neutron resonances in light nuclei. Another promising task is the intercomparison of excitation energies of isobaric analogue states in low mass isospin multiplets. Neutron experiments of the present type could provide part of the precise energy determinations necessary to study the A-, T-, Z- and N-dependence of nuclear binding energies and to solve basic problems such as a possible charge dependence of the nuclear forces[24-26]). In addition, the high energy resolution provides a convenient tool for the precise determination of total and partial widths of narrow states e.g., of isospin-forbidden resonances. These yield additional important experimental information on nuclear structure and the effective interaction matrix elements as well as more subtle electromagnetic effects in the nuclear states.

The authors are indebted to Dr. H. Schweickert for active assistance and helpful advice during the installation of the improved set-up. The assistance and the close collaboration of the cyclotron group, headed by F. Schulz, is also gratefully acknowledged.

References

1) G. D. James, in *Neutron standards and applications*, ed., C. D. Bowman and A. D. Carlson (US Department of Commerce, NBS Special Publication 493, Oct. 1977) p. 319 ff.
2) J. W. Meadows, NSE **49** (1972) 310; H. H. Knitter and C. Budtz-Jørgensen, Proc. Int. Conf. on *Interactions of neutrons with nuclei*, Lowell, Vol. II, (1976) p. 1387.
3) J. C. Davis and F. T. Noda, Nucl. Phys. **A134** (1969) 361.
4) A. H. Wapstra and K. Bos, At. Data Nucl. Data Tables **19** (1977) 175.
5) S. Cierjacks, B. Duelli, P. Forti, D. Kopsch, L. Kropp, M. Lösel, J. Nebe, H. Schweickert and H. Unseld, Rev. Sci. Instr. **39** (1968) 1249.
6) S. Cierjacks, in *Nuclear structure studies with neutrons*, eds., J. Erö and J. Szücs (Plenum Press, London, 1974) p. 299 ff.
7) W. Kneis, W. Kappel, B. Kögel, Ch. Lehmann, E. Leinweber, J. Möllenbeck, W. Segnitz and H. Schweickert, Proc. 8th Int. Conf. *Cyclotrons and their applications*, Indiana, USA,

1978, IEEE Trans. Nucl. Sci. NS-26 (1979) 2366.
[8]) K. D. Frohme and R. H. Bradsell, J. Sci. Instr. **43** (1966) 129; M. Kerner, VI Int. Course for *High precision length measurements,* Graz, Austria, 1970.
[9]) B. Meier-Hirmer, Allg. Verm. Nach **11** (1975) 373.
[10]) G. W. Schweimer, Nucl. Phys. **A100** (1967) 537.
[11]) I. de Lotto, E. Gatti and F. Vaghi, Proc. Int. Conf. on *Automatic acquisition and reduction of nuclear data,* eds., K. H. Beckurts, W. Gläser and G. Krüger, Karlsruhe (1964) p. 291 ff.
[12]) J. A. Young and J. U. Koppel, J. Chem. Phys. **42** (1965) 357.
[13]) R. Nicklow, N. Wakabayashi and H. G. Smith, Phys. Rev. **B5** (1972) 4951.
[14]) G. Breit and E. P. Wigner, Phys. Rev. **49** (1936) 519.
[15]) W. J. Thompson, J. L. Adams and D. Robson, Phys. Rev. **173** (1968) 975.
[16]) F. W. K. Firk, J. E. Lynn and M. C. Moxon, Proc. Phys. Soc. **82** (1963) 477.
[17]) F. Hinterberger, P. v. Rossen, H. G. Ehrlich, B. Schüller, R. Jahn, J. Bisping and G. Welp, Nucl. Phys. **A253** (1975) 125.
[18]) H. Derrien, Report NEANDC (E)-164-L, unpublished.
[19]) F. Ajzenberg-Selove, Nucl. Phys. **A281** (1977) 1.
[20]) F. Ajzenberg-Selove, Nucl. Phys. **A268** (1976) 1.
[21]) A. B. McDonald, T. K. Alexander and O. Häusser, Nucl. Phys. **A273** (1976) 464.
[22]) C. Detraz and H. H. Duhm, Phys. Lett. **29B** (1969) 29.
[23]) M. C. Lemaire, M. C. Mermaz and K. K. Seth, Phys. Rev. **C5** (1972) 328.
[24]) A. Arima and S. Yoshida, Nucl. Phys. **A161** (1971) 492.
[25]) H. Sato and S. Yoshida, Nucl. Phys. **A211** (1973) 509.
[26]) J. Jänecke, in *Isospin in nuclear physics*, ed., D. H. Wilkinson (North-Holland, Amsterdam, 1969) p. 297 ff.